HOSTED BY

ELSEVIER

CrossMark

Available online at www.sciencedirect.com

ScienceDirect

Progress in Natural Science: Materials International 26 (2016) 69–77

Progress in Natural Science Materials International

www.elsevier.com/locate/pnsmi
www.sciencedirect.com

Original Research

Effects of friction stir processing on the microstructure and superplasticity of in situ nano-ZrB_2/2024Al composite

Yutao Zhao*, Xizhou Kai, Gang Chen, Weili Lin, Chunmei Wang

School of Material Science and Engineering, Jiangsu University, Zhenjiang 212013, China

Received 20 July 2015; accepted 2 November 2015
Available online 23 February 2016

Abstract

In this study, in situ nano-ZrB_2/2024Al composites fabricated from 2024Al–K_2ZrF_6–KBF_4 system were processed by friction stir processing (FSP) to achieve superplasticity of the composites. And the effects of particle contents (1 wt%, 3 wt%, 5 wt%), matrix grain size (micron or submicron), strain rates ($5\times10^{-3}\ s^{-1}$, $1\times10^{-2}\ s^{-1}$, $2\times10^{-2}\ s^{-1}$) and deformation temperatures (400 K, 480 K, 600 K, 700 K, 750 K) on the superplasticity of the composites were investigated. After the friction stir processing, the coarse grains of the cast composites with matrix grain size of about 80–100 μm and nano-ZrB_2 reinforcement size of 30–100 nm were crushed into small grains about 1 μm in size, and the uniformity of the nano-ZrB_2 reinforcements was also improved. And under the same superplastic tensile testing condition at the temperature of 750 K and strain rate of $5\times10^{-3}\ s^{-1}$, the FSP nano 3 wt%ZrB_2/2024Al composite exhibited an superplastic elongation of 292.5%, while the elongation of the corresponding cast composite was only less than 100%. Meanwhile, the *m* values of the FSP composites were always higher than the cast composites, especially the FSP composites with 3 wt% particles has the *m* value of 0.5321 i.e., the FSP composites should had better superplastic properties than cast ones. Furthermore, the FSP composites had higher apparent deformation activation energy (*Q*) than that of the lattice diffusion of pure aluminium, indicating that the deformation mechanisms of the FSP composites should be grain boundary sliding mechanisms.

Keywords: In situ nano-ZrB_2/2024Al composite; Friction stir processing; Superplasticity; Deformation mechanism

1. Introduction

With high specific strength, high specific modulus, good wear resistance and good thermostability, particle-reinforced aluminum matrix composites (PRAMCs) have been widely used in the fields of aerospace, military, transportation and electronic packaging [1–4]. However, with the introduction of the reinforcement particles, the plasticity and toughness of the composites decreased dramatically, and lead to difficulty in parts forming, especially for the complex components. As a result, the superplastic deformation, especially the superplasticity with high strain rates ($\dot{\varepsilon}\geq10^{-2}\ s^{-1}$) of the PRAMCs has attracted great attention of the scientists. Nevertheless, the traditional PRAMCs are always difficult to achieve superplasticity, due to the large scale of the reinforcement particles and matrix grains [5–7]. On the one hand, the sharp-angled ceramic reinforcements of the traditional PRAMCs fabricated by exterior methods are always larger than 1 μm, which cannot deform and lead to stress concentration and cracks easily during the deformation, and hence result in early fracture of the composites. On the other hand, the traditional PRAMCs fabricated by powder metallurgy [5] or squeeze casting [6] exhibit a matrix grain size of larger than 10 μm, which cannot meet the key factor of superplasticity, that the grain size should be smaller than 10 μm [7–9].

In this study, the in situ technology was employed to fabricate nano-ZrB_2/2024Al composites from 2024Al–K_2ZrF_6–KBF_4 system, which has been proved to be a feasible strategy for mass production of nanoparticle reinforced aluminum matrix composites, where the composites with small reinforcements, such as the nanoparticles, always exhibit much more improvement in strength with little sacrifice of ductility [10]. At the same time, the friction stir processing was further

*Corresponding author. Tel.: +86 051188797900.
E-mail address: zhaoyt@ujs.edu.cn (Y. Zhao).
Peer review under responsibility of Chinese Materials Research Society.

http://dx.doi.org/10.1016/j.pnsc.2016.01.009

Table 1
Chemical constituents of 2024Al (mass fraction, %).

Si	Fe	Cu	Mn	Mg	Cr	Zn	Al
0.50	0.50	3.8–4.9	0.30–1.0	1.2–1.8	0.10	0.25	Bal.

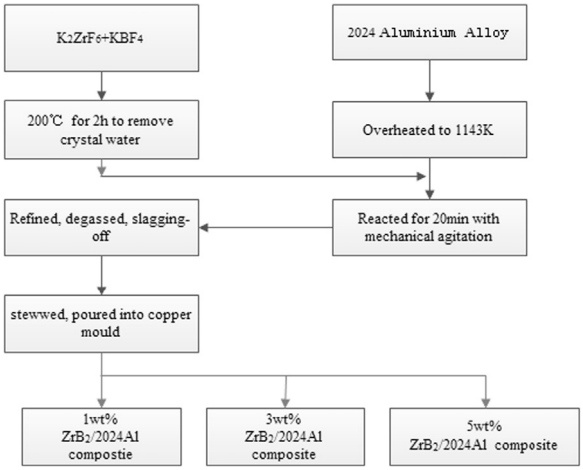

Fig. 1. Fabricating process of ZrB_2/2024Al composite from 2024Al–K_2ZrF_6–KBF_4 reaction system.

used to refine matrix grains and improve the uniformity of the in situ nanoparticles to achieve superplasticity of the composites. And the effects of particle contents, matrix grain size, strain rates and deformation temperatures of the composites on the superplastic properties were investigated in detail.

2. Experiments

The raw materials of the composites were 2024Al, K_2ZrF_6 and KBF_4 powders. Table 1 shows the element content of 2024Al alloy. In order to avoid the explosion hazard induced by crystal water of the powders or the adsorptive water vapor of the air on the powder surface, the K_2ZrF_6 and KBF_4 reactant powders were dehydrated at 573 K for 3 h firstly. Then the dried mixture powders were added to the molten 2024Al alloy at 1143 K for the in situ synthesis of ZrB_2 reinforcements, where the mass ratio of K_2ZrF_6 and KBF_4 was 52:48, an excess of KBF_4 to avoid the generation of Al_3Zr phase. After the in situ reaction, about 20 min, C_2Cl_6 was used to degas and purify the composite melt, and then the composite melt was cooled to about 993 K and pour to the copper mold to obtain the ZrB_2/2024Al composites. Fig.1 shows the fabricating process of the composites.

The cast composites was then machined to sheets with 4 mm in thickness for the friction stir processing (FSP) on a FSW-3LM-002 gantry friction stir welding machine. And the size of the stir-welding head and FSP parameters are listed in Tables 2 and 3, respectively.

The composition and microstructure of the fabricated composites were characterized by X-ray diffraction (XRD), optical microscopy (OM), scanning electron microscope (SEM), transmission electron microscope (TEM) and high-resolution TEM (HRTEM). And the high temperature tensile test was carried out on an S-2000X material testing machine, where the tensile test specimens were machined according to GB/T 2039-1997.

Table 2
Size of stir-welding head.

Shoulder diameter (mm)	Bottom diameter of stir pin (mm)	Head diameter of stir pin (mm)	Length of sir pin (mm)	Thread direction
12	5	4	3.7	Left-hand thread

Table 3
Technological parameters of FSP process.

Rotate speed (r/min)	Movement speed (mm/min)	Press amount (mm)	Tilt angle of stir head (°)	Type of the stir head
1000	70	3.75	2.5	Thread head

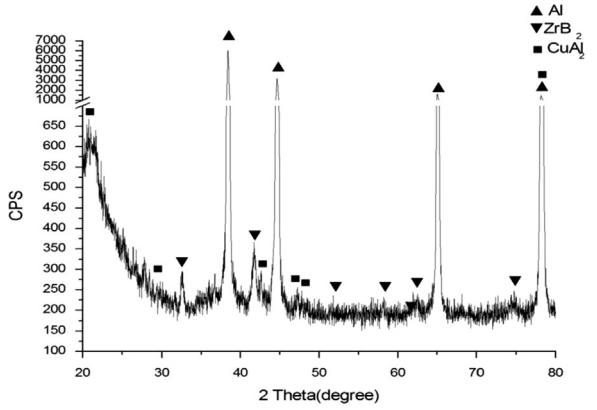

Fig. 2. XRD pattern of the fabricated 5 vol% ZrB_2/2024Al composite.

3. Results and discussion

3.1. Characterization of the cast composites

The possible chemical reactions of the Al–K_2ZrF_6–KBF_4 system are as follows [10,11]:

$$2KBF_4 + 3Al = AlB_2 + 2KAlF_4 \quad (1)$$

$$3K_2ZrF_6 + 13Al = 3Al_3Zr + K_3AlF_6 + 3KAlF_4 \quad (2)$$

$$AlB_2 + Al_3Zr = ZrB_2 + 4Al \quad (3)$$

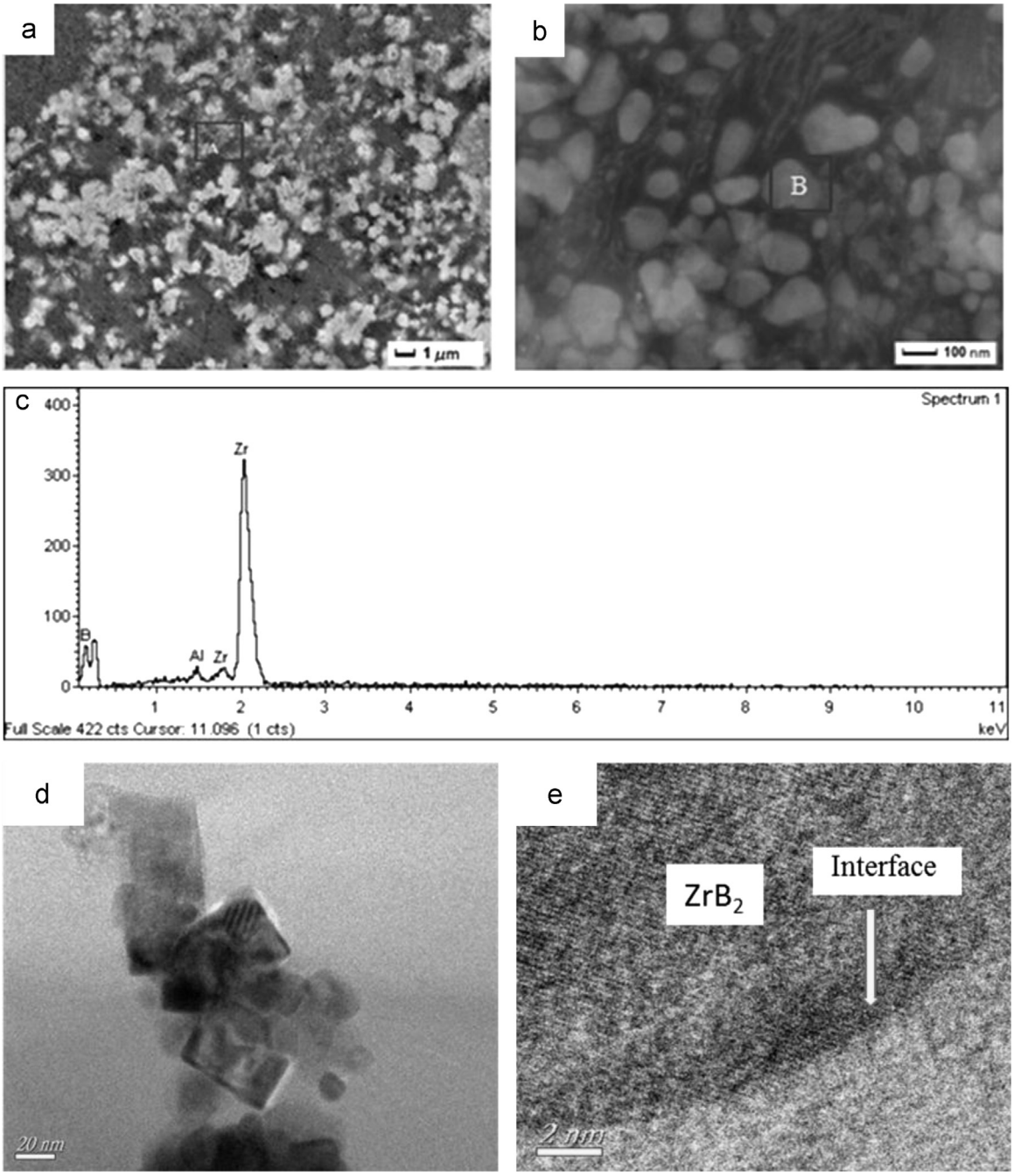

Fig. 3. SEM (a and b), EDS pattern (c), TEM (d) and HRTEM images (e) of the 5 vol% ZrB_2/2024Al composite.

Where the $KAlF_4$ and K_3AlF_6 are oily liquids above the alloy melt, and can be removed with slags after the reactions. Fig. 2 shows the XRD pattern of the in situ 5 vol% ZrB_2/2024Al composite fabricated from Al–K_2ZrF_6–KBF_4 system. The diffraction peaks of Al, $CuAl_2$, and ZrB_2 phases are all observable. And there are no peaks of Al_3Zr phase due to the excess of B element (KBF_4). And the total reaction in this study can be expressed as:

$$3K_2ZrF_6+6KBF_4+10Al=3ZrB_2+9KAlF_4+K_3AlF_6 \quad (4)$$

Fig.3 shows SEM, TEM, and EDS images of the 5 vol% ZrB_2/2024Al composite. As shown in Fig. 4a and b, the reinforcement particles are mostly rectangular or nearly hexagonal with size from 30 to 100 nm in diameter. Combining the EDS analysis of the reinforcement which is mainly composed of Zr and B elements shown in Fig. 3c, and the XRD analysis of the composite in Fig.3, these nanoparticles should be ZrB_2. Fig. 3d shows the TEM image of the in situ ZrB_2 nanoparticles. And Fig. 3e shows the HRTEM image around the interface of the ZrB_2 and Al matrix. It can be seen that the in situ nano-ZrB_2 and Al matrix have a good and clean interface bonding without any inclusions or intermediate products.

Fig. 4 shows the optical micrographs of 2024Al alloy and in situ nano-ZrB_2/2024Al composites. It can be seen that the cast

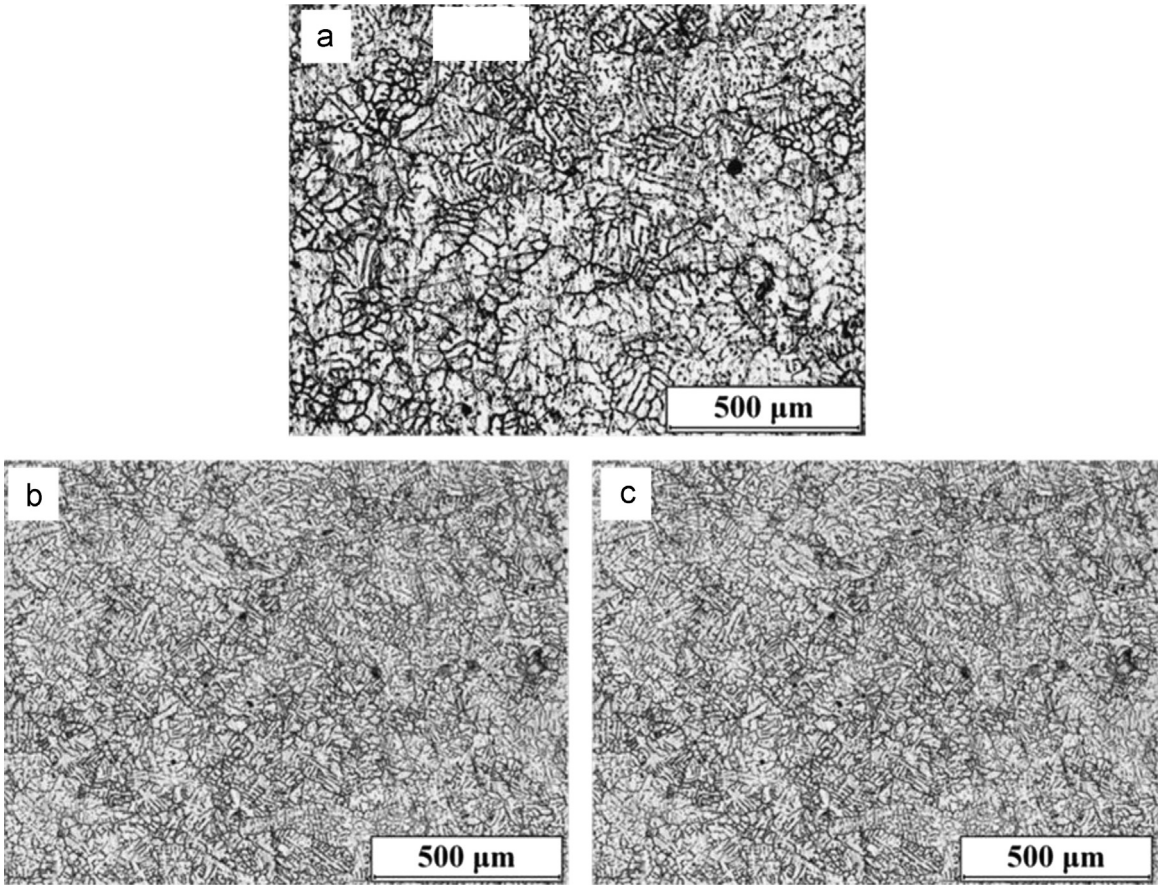

Fig. 4. OM images of the 2024Al (a) and the nano-ZrB_2/2024Al composites with different content of ZrB_2 reinforcement: (b) 3 wt%, (c) 5 wt%.

2024Al alloy exhibits a coarse and dendritic grain microstructure, shown in Fig. 5a. However, with the introduction of in situ nano-ZrB_2 reinforcement particles, the matrix of the composites exhibit a thin and small dendritic grain microstructure as shown in Fig. 5b and c, due to the grain-refine effects of the in situ nano-sized ZrB_2 particles [11–13].

3.2. Microstructures of the FSP composites

Fig. 5 shows the macrograph of the cross section, perpendicular to the FSP deformation direction of the composites. It can be seen that the composite in FSP zone been well refined. In fact, the materials in the FSP zone are in semi-solid states during the friction stir processing and subjected to severe plastic deformation, due to the temperature rising induced by both the stirring of the processing head and the mechanical shear stress of the high-speed rotational stirring head. Finally, the reinforcement particles of the composites in FSP zone were redistributed uniformly and the matrix grain size of the composites were refined dramatically. Fig. 5b and c show the OM images of the zone marked in Fig.5a. Fig.5b is the typical structure of the cast composites, and Fig.5c is the characteristic of the structure of FSP composites, showing a dramatic structure refinement compared with the corresponding cast one. SEM images of composites before and after FSP, shown in Fig. 5d and e, indicate that the clusters of nanoreinforcements are well broken and the reinforcements distribute uniformly in the matrix.

And this uniformity improvement of the in situ nanoparticles can also be seen from the TEM images of the composites before and after FSP shown in Fig. 6. The in situ ZrB_2 particles of the cast composites are always agglomerated in local area, shown in Fig. 5d and Fig. 6a. However, the in situ ZrB_2 particles of the FSP composites distribute uniformly shown in Fig. 6b, which should be benefit for the mechanical improvement, especially for the ductility enhancement of the metal matrix nanocomposites.

3.3. Superplastic properties of the FSP composites

Fig. 7 shows the tensile specimens of the 3 wt% ZrB_2/2024Al composites at the temperature of 750 K and strain rate of $5 \times 10^{-3}\ s^{-1}$. It can be seen that the FSP composite exhibits an elongation of 292.5%, while the corresponding cast composite only deformed to failure at 62.9%. From the structure analysis of the composites in Section 3.2, we can know that this superplastic property improvement of the FSP composite should be attributed to the grain refinement and uniform distribution of the nanoparticles. And the early researches have shown that thermally-stable small grains and uniform distribution of reinforced phases are the key factors to achieve superior superplasticity of metallic materials.

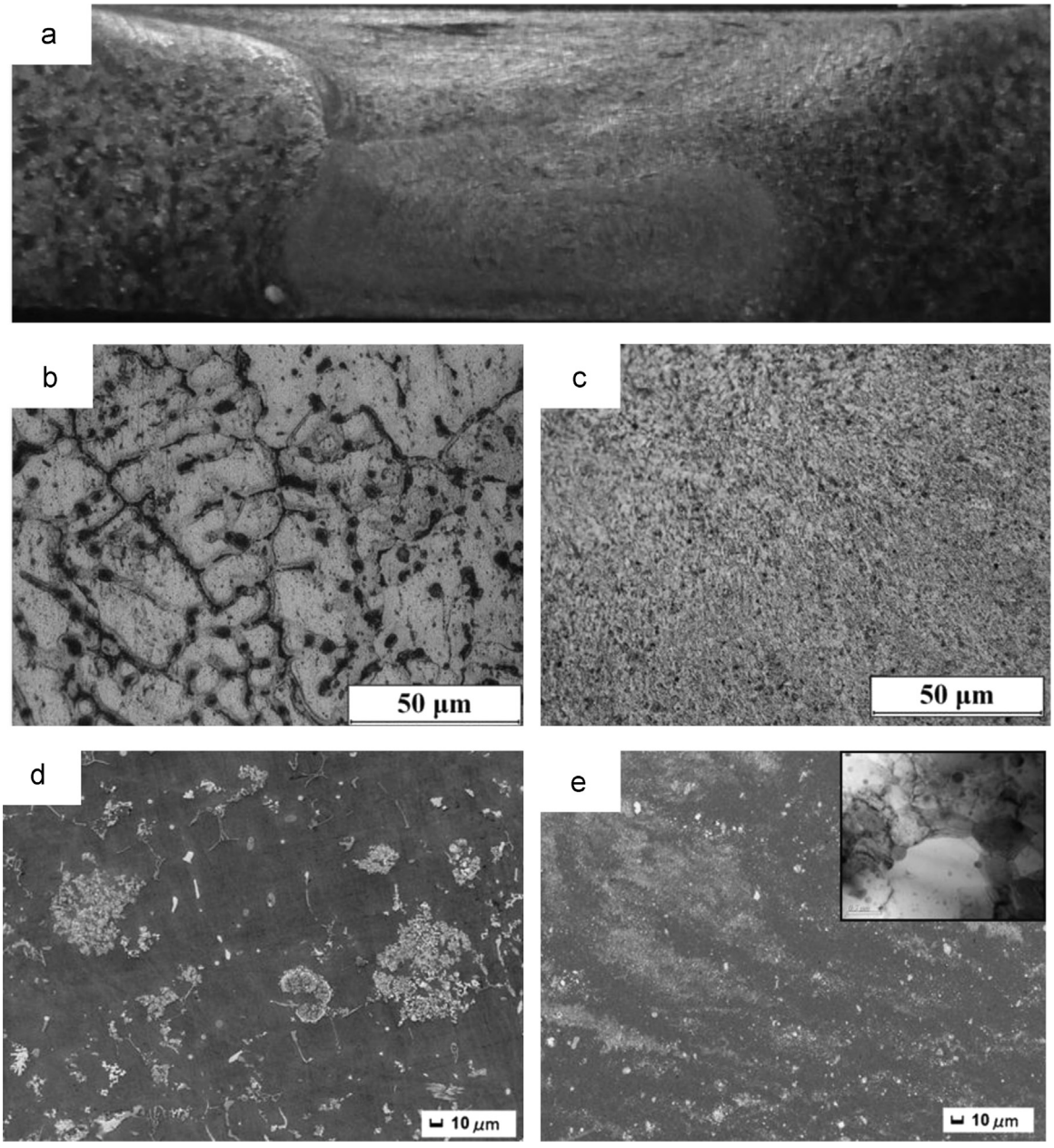

Fig. 5. (a) Cross-sectional macrograph of composites after FSP process and images of the composites before (OM: b, SEM: d) and after (OM: c, SEM: e) FSP process.

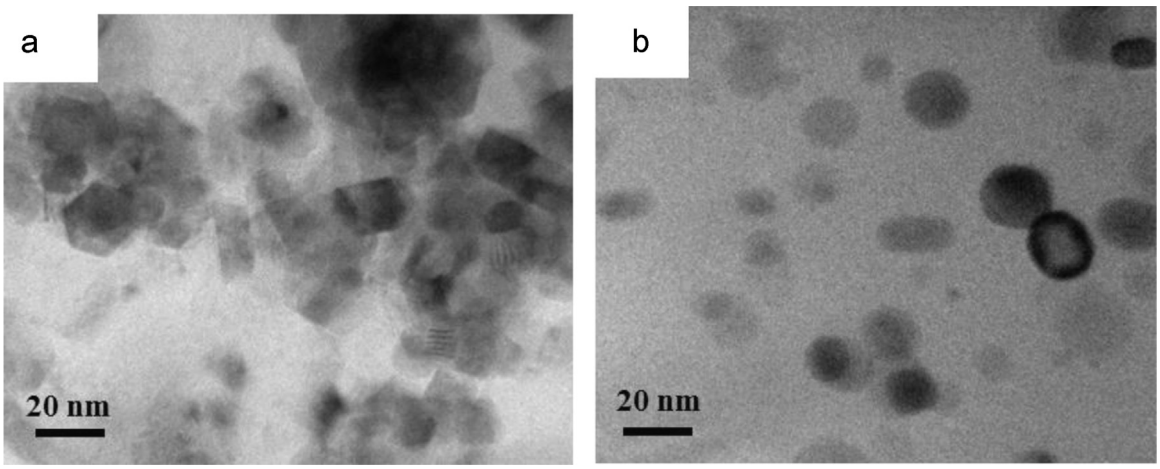

Fig. 6. TEM images of reinforcements before (a) and after (b) FSP process.

It is well known that the extrinsic factors of temperature and initial strain rates are also the essential conditions for superplastic deformation of the materials. Fig. 8 shows the true stress-true strain curves of the FSP ZrB_2/2024Al composites with different content of ZrB_2 reinforcement at different test temperatures for the given stain rate of 0.01 s^{-1}. It can be easily seen that with the increasing of the deformation temperature, the elongation increased and the stress decreased. However, for the same deformation condition, the 3 wt% ZrB_2/2024Al composite exhibited the largest elongation, where the high content of agglomerated in situ nano-ZrB_2 particles in 5 wt% ZrB_2/2024Al composite should be the key factor for the elongation decreasing compared with the 3 wt% ZrB_2/2024Al composite.

The strain rate sensitivity factor, *m*, represents the ability of the composite to resist necking during deformation and is usually used as the criterion for the superplasticity of materials.

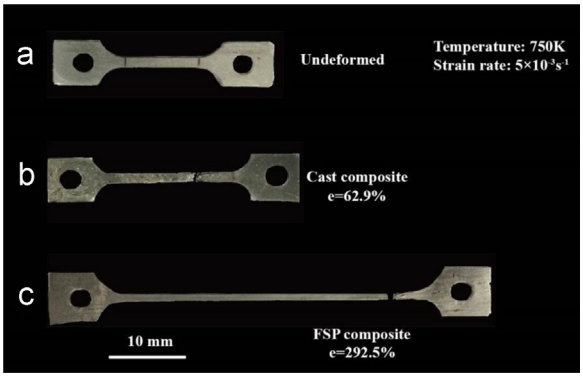

Fig. 7. Tensile specimens of the 3 wt% ZrB_2/2024Al composites at temperature of 750 K and strain rate of 5×10^{-3} s^{-1}: (a) undeformed, (b) cast composite and (c) FSP composite.

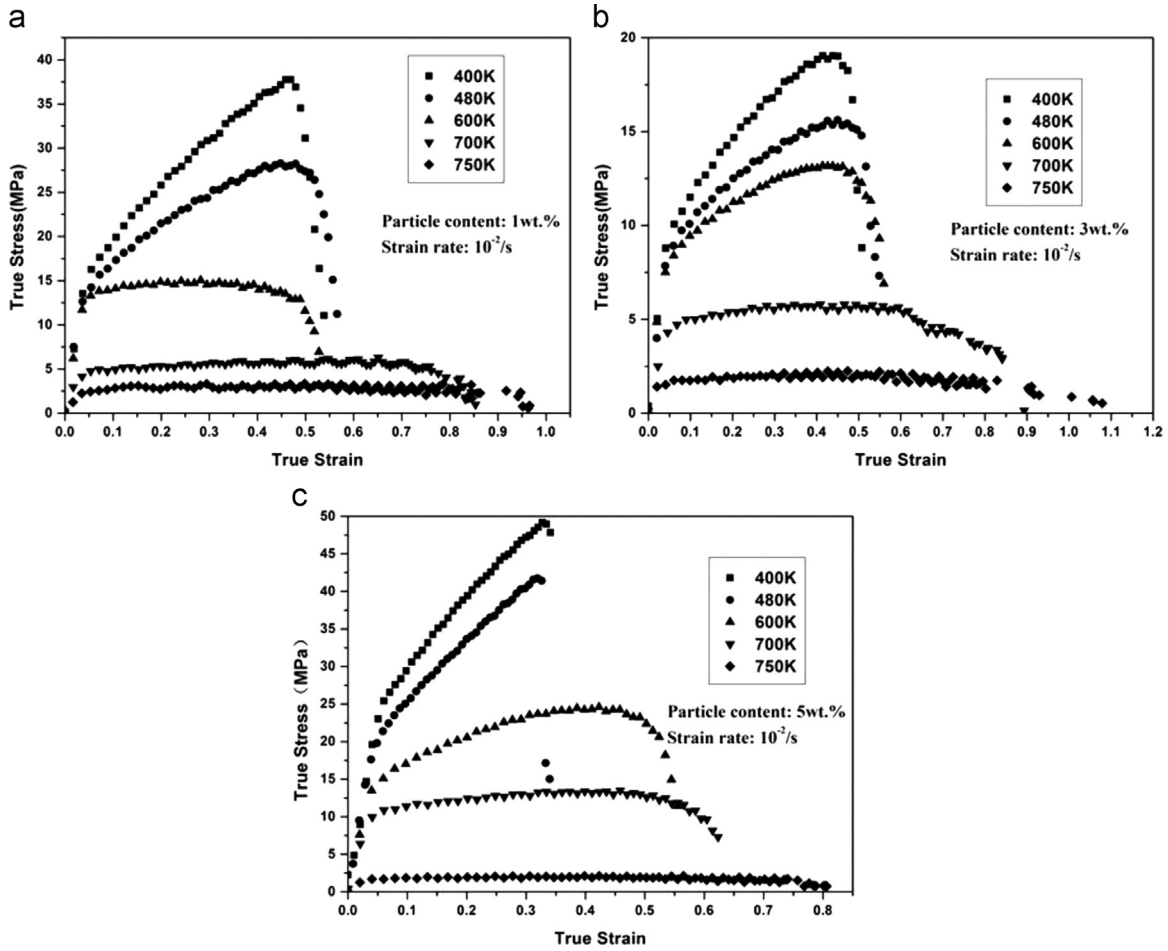

Fig. 8. True stress-true strain curves of the FSP ZrB_2/2024Al composites with different content of ZrB_2 reinforcements at different test temperatures for the given stain rate of 0.01 s^{-1}: (a) 1 wt%, (b) 3 wt% and (c) 5 wt%.

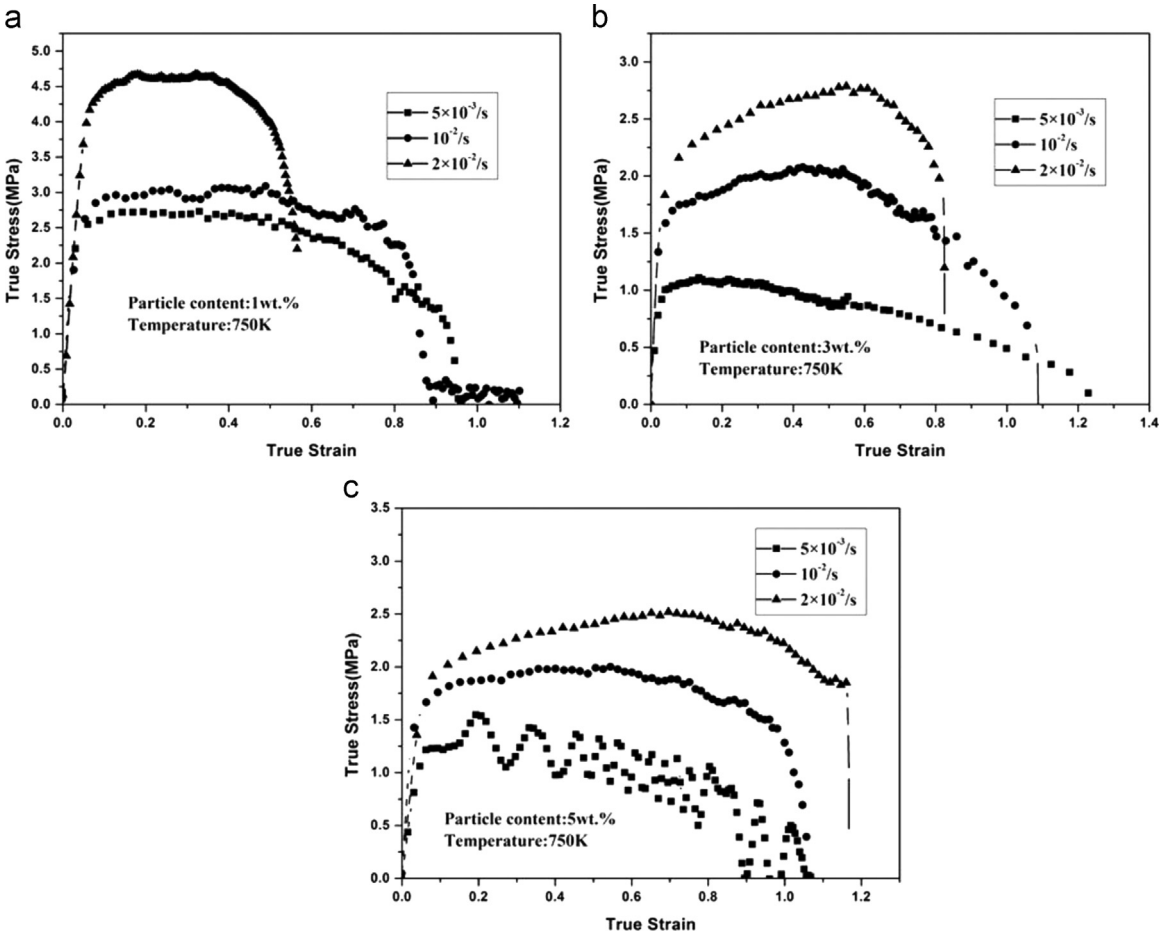

Fig. 9. True stress–true strain curves of different composites after FSP under different strain rate: (a) 1 wt%, (b) 3 wt% and (c) 5 wt%.

Here, the high-temperature flow stress (σ) of superplastic materials can be related to the strain rate ($\dot{\varepsilon}$) by a power-law relationship as:

$$\sigma = K\varepsilon^n \dot{\varepsilon}^m \tag{5}$$

Where σ is the true stress, K is constant, ε is the true strain, $\dot{\varepsilon}$ is the train rate, and m is the strain rate sensitivity factor. Taking logarithm of Eq. (5) on both sides, the m can be determined to be:

$$m = \frac{d \ln \sigma}{d \ln \dot{\varepsilon}} \tag{6}$$

With the data of the true stain–true stress curves under different strain rates, shown in Fig. 9, the ln$\dot{\varepsilon}$–lnσ curves could be obtained as Fig. 10 and the slopes of the curves would be the values of m. To make sure the veracity of the m values, the range of the measured strain was located in the range of 0.2–0.5 in this study [14].

Fig. 10 shows the ln$\dot{\varepsilon}$–lnσ curves and the m values of the FSP composites at different true strains. It can be seen that the m values of the 3 wt% ZrB_2/2024Al composite and 5 wt% ZrB_2/2024Al composite are higher than that of 1 wt% ZrB_2/2024Al composite, which indicates that the introduction of the nanoparticles could improve the superpalsticity of the composites. And among the three composites, the 3 wt% ZrB_2/2024Al composite exhibits the largest m value, meaning best superplasticity, which is in accordance with the true stress–true strain curves. In addition, all the m values of the composites were higher than 0.3 at strain rate higher than 0.01 s^{-1}, so the in situ nano-ZrB_2/2024Al composites have good high strain rate superplastic properties.

The activation energy for a particular deformation process always gives an idea about the rate-controlling mechanism. Assuming that the deformation during high temperature tensile tests are thermally activated, the strain rate can be expressed as shown in Eq. (7), which is usually used to analyze the superplastic deformation mechanisms:

$$\dot{\varepsilon} = A\sigma^n \exp\left(-\frac{Q}{RT}\right) \tag{7}$$

Where $\dot{\varepsilon}$ is the strain rate, σ is the flow stress, Q was the deformation activation energy, A is a constant of the material, R is the gas diffusion constant, T is the absolute temperature, and n meant strain exponent, $n = 1/m$. And the Q value can be calculated as:

$$Q = \frac{1}{m} R \frac{\partial \ln \sigma}{\partial (1/T)} \tag{8}$$

Therefore, the thermal activation Q can be estimated from the slope of lnσ-1/T at a given value of $\dot{\varepsilon}$. Choosing the true strain of 0.3 as an example, according to the date of different temperatures and strain rates, the plot of lnσ–1000T^{-1} was established in

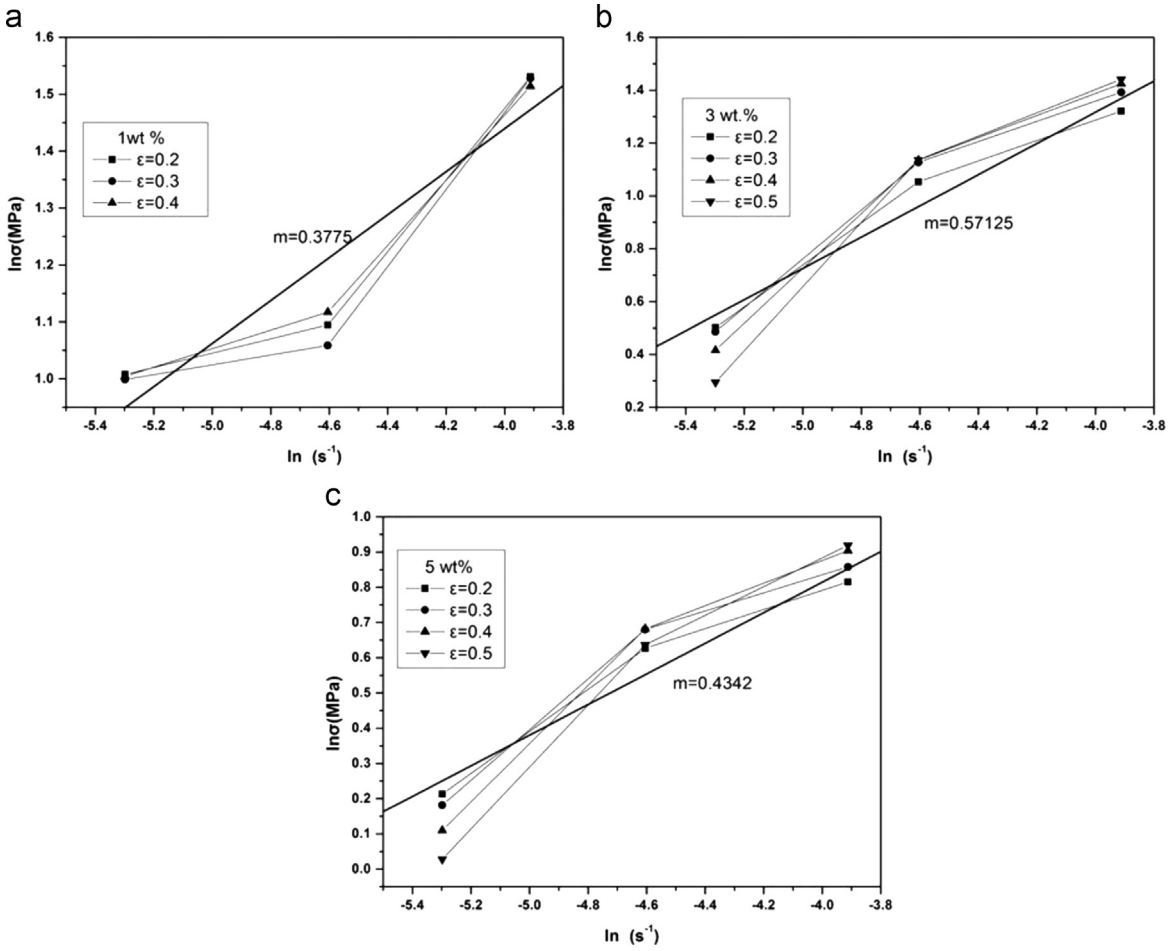

Fig. 10. $\ln\dot{\varepsilon}$–$\ln\sigma$ curves of the FSP composites at different true strains: (a) 1 wt%, (b) 3 wt% and (c) 5 wt%.

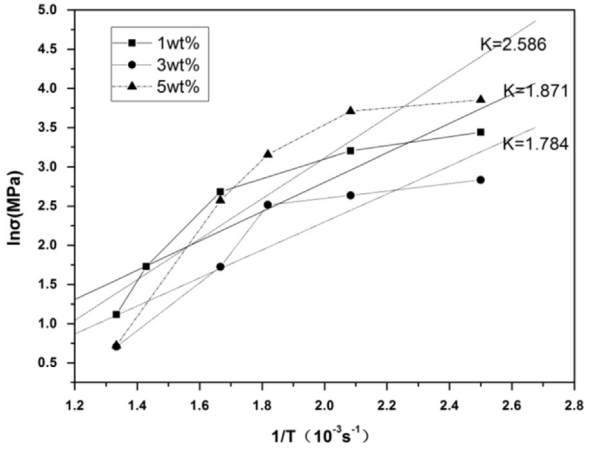

Fig. 11. $\mathrm{Ln}\sigma - 1000T^{-1}$ curves of the composites after FSP process.

Fig.11. And the activation energy Q was calculated to be 412, 279, and 498 kJ/mol for the 1 wt%, 2 wt% and 3 wt% ZrB_2/2024Al composites, respectively, which are all higher than that of the lattice diffusion activation energy of pure aluminum (142 kJ/mol). As a result, the deformation mechanism of the FSP composites should be the grain boundary sliding and dynamic recrystallization mechanisms, where a higher energy is needed compared with that of lattice diffusion mechanisms.

4. Conclusion

(1) The in situ nano-ZrB_2/2024 composites were successfully fabricated from 2024Al–K_2ZrF_6–KBF_4 system at 1143 K, The ZrB_2 particles showed hexagonal or square morphologies with average size between 30–100 nm. The introduction of ZrB_2 particles results in matrix grain refinement of the composites.

(2) Through the friction stir processing (FSP), the matrix grains were refined dramatically, and the agglomerated in situ synthesized nano-ZrB_2 particles were redistributed uniformly in the matrix. And the FSP composites exhibit better superplasticity than the corresponding cast ones. As a example, the FSP 3 wt% ZrB_2/2024Al composite exhibits an superplastic elongation of 292.5% under the test condition of 750 K and 5×10^{-3} s^{-1}, while the elongation of the corresponding cast composite was only less than 67.2%.

(3) The introduction of the nanoparticles could improve the m value, strain rate sensitivity factor, of the composites and result in the superplastic enhancement. However, the high content of nanoparticles is not benefit for the superplasticty due to the difficulty in uniform distribution of these nanoparticles.

(4) The deformation activation energy (Q) of FSP composites were estimated and are always higher than that of lattice diffusion of pure aluminum and indicate that the key deformation mechanisms of the FSP composites should be the grain boundary sliding and dynamic recrystallization mechanisms.

Acknowledgments

The authors would like to acknowledge the financial support of the National Natural Science Foundation of China (51174098), the Special Research Foundation of Doctoral Program in institutions of higher learning (20133227110023), Research Foundation for Advanced Talents of Jiangsu University (14JDG125), the Postdoctoral Science Foundation of Jiangsu Provincial (1501029B), and the Fourth '333' Project Research Foundation of Jiangsu Province (BRA2012135).

References

[1] G.R. Li, X.Y. Zhang, H.M. Wang, Y.T. Zhao, G. Chen, Z. Zhang, Univ. Sci. Technol. 34 (2012) 552–557.
[2] B. Kaveendran, G.S. Wang, L.J. Huang, et al., J. Alloy. Compd. 51 (2013) 16–22.
[3] I. Kerti, Mater. Lett. 59 (2005) 3795–3800.
[4] H.M. Zakaria, Ain Sham, Eng. J. 5 (2014) 831–838.
[5] Y. Birol, Trans. Nonferr. Met. Soc. China 25 (2015) 677–682.
[6] K. Asano, Mater. Manuf. (2015).
[7] A.R. Chezan, J.T. Hosson, Mater. Sci. Eng. A 410 (2005) 120–123.
[8] G.D. Bengough, Inst. Met. 7 (1912) 123–127.
[9] B. Abbasipour, B. Niroumand, S.M. Vaghefi, Trans. Nonferr. Met. Soc. China. 20 (2010) 1561–1566.
[10] X.Z. Kai, Y.T. Zhao, A.D. Wang, C.M. Wang, Z.M. Mao, Compos. Sci. Technol. 116 (2015) 1–8.
[11] G.R. Li, X.Y. Zhang, et al., Chin. J. Eng. 34 (2012) 552–557.
[12] P. Schumacher, A.L. Greer, et al., Green Mater. Sci. Technol. 14 (1998) 394–404.
[13] B.F. Schultz, J.B. Ferguson, P.K. Rohatgi, Mater. Sci. Eng. A 530 (2011) 87–97.
[14] G.C. Wang, C.X. Cao, H.B. Dong, et al., Acta Aeronaut. Astronaut. Sin 30 (2009) 357–361.